



## Observation and modeling of surface currents on the Grand Banks: A study of the wave effects on surface currents

C. L. Tang,<sup>1</sup> W. Perrie,<sup>1</sup> A. D. Jenkins,<sup>2</sup> B. M. DeTracey,<sup>1</sup> Y. Hu,<sup>1</sup> B. Toulany,<sup>1</sup>  
and P. C. Smith<sup>1</sup>

Received 23 November 2006; revised 15 May 2007; accepted 9 August 2007; published 31 October 2007.

[1] We investigate the effects of surface waves on surface currents using surface drifter data from the Grand Banks and a coupled current-wave-drifter model. The theoretical basis of the study is Jenkins' theory of wave-current interaction in which wind-generated surface currents are modified by wind-wave and wave-current momentum transfers. The total surface current is the sum of the wave modified current, the Stokes drift and the tidal current. Jenkins' formulation was incorporated into the Princeton Ocean Model and applied to the Labrador Sea and the adjacent shelves. The wave energy spectrum from Wavewatch III was used to calculate the momentum transfer and the Stokes drift. A series of model experiments were conducted to simulate the drifter trajectories and examine the sensitivity of the simulations to model parameters. The results show that the Stokes drift is the dominant wave effect, which increases the surface drift speeds by 35% and veers the currents toward the wind directions. The net effect of wind-to-wave and wave-to-current momentum transfers reduces the surface speeds by a few percent. A statistical analysis of the model currents and drifter data shows that the inclusion of the wave effects improves the model simulations significantly. Model errors due to uncertainties in the model parameters including the eddy viscosity, wave spectrum, air drag of the drifters, and bottom friction are investigated. The model surface currents are shown to be most sensitive to the surface eddy viscosity and the wave energy spectra.

**Citation:** Tang, C. L., W. Perrie, A. D. Jenkins, B. M. DeTracey, Y. Hu, B. Toulany, and P. C. Smith (2007), Observation and modeling of surface currents on the Grand Banks: A study of the wave effects on surface currents, *J. Geophys. Res.*, *112*, C10025, doi:10.1029/2006JC004028.

### 1. Introduction

[2] Ocean surface waves have long been known to give rise to near-surface drift currents, the strength of which, for small-amplitude irrotational waves, is proportional to the square of the wave slope [Stokes, 1847]. The definition of this Stokes drift is the mean velocity of fluid particles over a wave cycle, and for a single deep-water wave component, it decreases with depth as  $e^{2kz}$  (wave number  $\mathbf{k}$  with modulus  $k$ ). Irrotationality of surface waves is in principle violated on a rotating earth [Ursell, 1950] rendering it impossible for surface waves to set up a steady drift current in a frictionless ocean. This paradox was resolved by Hasselmann [1970], who showed that the Stokes drift would be combined with inertial oscillations in such a way that the time-averaged current would be zero, and Pollard [1970] found an elegant exact solution of the hydrodynamic equations in Lagrangian coordinates, combining inertial oscillations with rotationally modified Gerstner waves [Gerstner, 1804]. Jenkins [1986],

building on the Lagrangian-coordinate perturbation expansion approach of Chang [1969], Ünlüata and Mei [1970], and Weber [1983a, 1983b], showed how this Stokes drift solution combined with inertial oscillations would be modified in the presence of a small (eddy) viscosity.

[3] In addition to transporting energy, surface waves transport momentum which, to second order in the wave slope, is equal to the water density multiplied by the vertically integrated Stokes drift. The fact that the waves carry momentum means that when waves dissipate, by means of viscous forces, turbulence, and/or wave breaking, this momentum is transferred to the mean Eulerian current. (Although mechanical energy may be dissipated as heat, kinetic and potential energy may be exchanged via buoyancy processes, and buoyancy processes (gravity) may affect the vertical component of momentum, the horizontal components of the momentum are conserved under dissipative processes, being changed only by horizontal pressure gradients and the Coriolis acceleration.) This phenomenon is most obvious in the nearshore zone [e.g., Longuet-Higgins and Stewart, 1962; Thornton and Guza, 1986], but for dynamical consistency, it should also be taken into account in the open ocean. Longuet-Higgins [1953] showed that if waves were damped by a constant viscosity, this transfer of momentum would occur within a thin near-surface vorticity

<sup>1</sup>Bedford Institute of Oceanography, Ocean Sciences Division, Fisheries and Oceans Canada, Dartmouth, Nova Scotia, Canada.

<sup>2</sup>Geophysical Institute, University of Bergen and Bjerknes Centre for Climate Research, Bergen, Norway.

layer [Lamb, 1932], and act on the mean flow field as an additional shear stress at the upper boundary. Weber [1983a, 1983b] incorporated the effect of rotation into this analysis, and Jenkins [1986] showed how to include the effects of a spatially and temporally varying wavefield. Jenkins [1987] demonstrated that if waves were damped by the effect of a vertically varying eddy viscosity, the transfer of wave momentum to the current field would take place within the water column at a rate dependent on the eddy viscosity gradient, and he applied his results to couple a spectral wave model and a one-dimensional model for the vertical current profile [Jenkins, 1989]. An important result of Jenkins' investigations was that different eddy viscosities had to be used for the mean current motions and for wave dissipation: if the "current" eddy viscosity is used for wave damping, the wave damping is excessive, a result which is consistent with "rapid distortion" turbulence theory [Batchelor and Proudman, 1954; Townsend, 1976; Mastenbroek et al., 1996; Teixeira and Belcher, 2002]. This is because the timescale of the turbulent eddies which act on the mean flow is much greater than the timescales of the wave Fourier components. Of course, the idea that wave damping is caused by eddy viscosity is not necessarily realistic, but even if other processes such as wave breaking/whitecapping are dominant, it is necessary for dynamical consistency to transfer the wave momentum which is lost into the current field, either by means of a change in the surface boundary condition or as a source of momentum within the water column.

[4] The coordinate system employed near the sea surface in this paper is approximately Lagrangian with respect to the wave orbital motions. This is in the sense that the surface drift corresponds to the mean motion of fluid particles at the actual sea surface, and the drift at a depth  $-z$  corresponds to the mean velocity of fluid particles which are at a mean distance  $z$  from the surface, even though that distance may be less than the surface wave amplitude. On the other hand, the coordinate system is approximately Eulerian with respect to the longer-term mean motions, since it does not move with the current. One such hybrid Lagrangian/Eulerian coordinate system, the generalized Lagrangian mean (GLM) framework, was rigorously derived by Andrews and McIntyre [1978a, 1978b], and applied to the problem of surface waves by a number of authors [Grimshaw, 1981; Craik, 1982; Groeneweg and Klopman, 1998; Groeneweg and Battjes, 2003]. To second order in wave slope and for short times, the Lagrangian coordinate perturbation expansion employed by Weber [1983a, 1983b] and Jenkins [1986, 1987, 1989] will give approximately the same mean-flow equations as the GLM approach. The system of equations which we introduce in section 2.1 may be regarded as being approximately GLM, subject to the following approximations: (1) the continuity equation differs from that of GLM, as we neglect the second-order change that the latter method induces in the GLM-Eulerian coordinate transformation Jacobian, and as a result, the mean surface elevation differs slightly from that obtained with the GLM method; and (2) the random-phase approximation used for the wavefield violates the projection property of the averaging procedure used in the GLM theorems.

[5] The transport of momentum by the wavefield may also be described in terms of the radiation stress associated with the wavefield, described for surface gravity waves by Longuet-Higgins and Stewart [1960, 1962] and discussed more recently by McWilliams et al. [1997], Ardhuin et al. [2003], Mellor [2003], and Jenkins and Ardhuin [2004]. For regular waves propagating in the  $x$  direction, their horizontal momentum flux in the direction of propagation is, to second order in the wave slope, given by the  $xx$  component of the radiation stress,

$$S_{xx} = EC_g/C, \quad (1)$$

where  $E = \rho_o g H^2/8$  is the wave energy,  $C_g$  is the group speed and  $C$  is the phase speed ( $H$  is the significant wave height,  $\rho_o$  is the water density and  $g$  is the acceleration due to gravity).

[6] An interesting study of the radiation stress and momentum balance in wind waves is reported by Mitsuyasu [1985], who showed that the spatial rate of growth of wave momentum in deep water, to second order in wave steepness  $kH/2\pi$ , is given by

$$(dS_{xx}/dx)|_{\text{wind input}} \approx 220(kH/2\pi)^2 T_a, \quad (2)$$

in the absence of time-dependent effects, nonlinear wave-wave interaction and wave energy dissipation. In (2),  $S_{xx}$  is the wave radiation stress (wave momentum transported per unit time across a unit line segment), and  $T_a$  is the wind stress. This result is based on laboratory measurements [Mitsuyasu and Honda, 1982], which give  $b/f = 0.34(u_*/C)^2$ , where  $b$  is the wave exponential growth rate,  $f$  is the wave frequency, and the wind friction velocity  $u_*$  is equal to  $(T_a/\rho_a)^{1/2}$ , where  $\rho_a$  is the air density. According to (2), as the wave steepness approaches 0.07, the proportion of the applied wind stress transferred to the waves will approach 100%. Assuming that the wave directional energy distribution is proportional to  $\cos 2\eta$  ( $\eta$  is the angle with respect to the wind direction), and using Mitsuyasu's [1968] relation,  $g^2 E/u_*^4 = 1.72 \times 10^{-4} (gx/u_*^2)\rho_o g$ , for the fetch dependence of wave energy, Mitsuyasu [1985] found that in wind-generated waves,

$$dS_{xx}/dx|_{\text{total}} \approx (3/8)dE/dx \approx 5.4 \times 10^{-2} T_a, \quad (3)$$

so that only about 5% of the applied wind stress is advected away by growing wind waves. Therefore, there should be a rough overall balance between the applied wind stress and the flux of momentum.

[7] Csanady [1984] proposed a shear layer at the surface analogous to a wall layer. A major difference between this shear layer and the wall layer is that the former uses a much larger roughness parameter, arising presumably from direct energy input to surface turbulence by the wind. Velocity gradients near the free surface are much smaller than those next to a solid wall under otherwise comparable conditions.

[8] To study the impact of waves on surface currents, Perrie et al. [2003] coupled the formulation of Jenkins [1986, 1987, 1989] to a simple linear diagnostic ocean

model with an Ekman layer and a depth-independent eddy viscosity. They showed that the wave effect could increase the surface currents by as much as 40%. In this paper, we follow the methodology developed by *Perrie et al.* [2003] and use advanced ocean and wave models to compute wind-driven currents and wave spectrum. The purpose is to obtain an improved estimate of the wave effects on surface currents. Jenkins' formulation is implemented in the Princeton Ocean Model (POM) and applied to the Labrador Sea and the Labrador/Newfoundland shelves. A wave model, Wavewatch III, is used to calculate the Stokes drift and momentum transfers among winds, waves and currents. Four surface drifters deployed on the Grand Banks in October 2002 provide a test data set. To account for the air drag on the drifters, a drifter model is used to correct for the observed surface currents. Although the ocean, wave and drifter models all have adjustable parameters, no attempt was made to optimize them in this paper, with respect to the comparison with observations. Rather, the approach is to use a standard set of ocean and wave parameters in the models within their allowable ranges to obtain reasonably representative surface currents. Wave effects are then studied by comparing the model simulations including waves, to simulations with no waves. Uncertainties in the model parameters are examined from a sensitivity analysis. The timescales of interest in this paper are from a few hours to several days. Surface currents of longer timescales are dominated by ocean processes that are not related to waves.

[9] The paper is organized as follows. Section 2 presents the current-wave and current-drifter coupling schemes. Section 3 is a description of the ocean and wave models used in the simulations. Wind and surface drifter data are described in section 4. In section 5, an analysis of the drifter data is presented and the results are compared to baseline model simulations. Section 6 discusses the properties of the Stokes drift. Section 7 is a sensitivity study of the model parameters. Section 8 presents the conclusions.

## 2. Current-Wave and Current-Drifter Coupling

[10] The computation of surface currents involves both the wave and ocean dynamics. The governing equations for surface currents are a set of Navier-Stokes equations modified by waves. The wave spectrum and the solution of the modified Navier-Stokes equations are obtained from a wave model and a 3-D circulation model described in section 3. To compare the model surface currents with velocities derived from surface drifters, knowledge of the response of the drifters to air drag is required. A simple model of a surface drifter is developed in section 2.2 to calculate the correction of drifter velocities due to the air drag.

### 2.1. Current-Wave Coupling

[11] Ocean currents with timescales of variability much longer than the wave periods can be written as the sum of three terms,

$$\mathbf{U} = \mathbf{u}_s + \mathbf{u}_t + \mathbf{u}, \quad (4)$$

where  $\mathbf{u}_s$  is the Stokes drift,  $\mathbf{u}_t$  is the tidal current and  $\mathbf{u}$  is the Eulerian mean current [*Huang, 1971*];  $\mathbf{u}_s$  can be

computed from 2-dimensional wave energy spectrum,  $E(f, \theta)$ , by

$$\mathbf{u}_s = 4\pi \int \int f \mathbf{k} e^{2kz} E(f, \theta) df d\theta, \quad (5)$$

where  $f$  is wave frequency and  $\theta$  is wave direction. The wave spectrum,  $E(f, \theta)$ , is governed by the wave energy equation [*Komen et al., 1994*]

$$\frac{\partial E(f, \theta)}{\partial t} + \mathbf{C}_g \cdot \nabla E(f, \theta) = S_{in} + S_{ds} + S_{nl}, \quad (6)$$

where  $\mathbf{C}_g$  is the group velocity of waves.  $S_{in}$ ,  $S_{ds}$  and  $S_{nl}$  are the source terms for wave generation, dissipation and nonlinear energy transfer, respectively. We assume that the deep-water dispersion relation applies for surface gravity waves, and neglect the effect of ocean currents on wave propagation as a higher-order effect, so that (6) is valid for wave energy.

[12] The tidal current,  $\mathbf{u}_t$ , was calculated from a barotropic tidal model for the eastern Canadian shelves [*Han et al., 1996; Han, 2000*]. The model includes major semidiurnal ( $M_2, S_2, N_2$ ) and diurnal ( $K_1, O_1$ ) tides.

[13] The Eulerian mean current,  $\mathbf{u}$ , is governed by a set of modified Navier-Stokes equations,

$$\frac{d\mathbf{u}}{dt} + \mathbf{f} \times (\mathbf{u} + \mathbf{u}_s) = -\frac{1}{\rho_o} \nabla p + \frac{\partial}{\partial z} \left( K_m \frac{\partial \mathbf{u}}{\partial z} \right) + \mathbf{u}_s \times \boldsymbol{\omega} + \mathbf{F}_{ds}, \quad (7)$$

$$\nabla \cdot \mathbf{u} + \frac{\partial w}{\partial z} = 0, \quad (8)$$

$$p = g\rho_o\zeta + g \int \rho dz + p_{air} + p_g, \quad (9)$$

where  $\mathbf{u}$  is also denoted as the quasi-Eulerian current [*Jenkins, 1986*] since it also refers to the quasi-Lagrangian mean fluid particle positions. In (7),  $\mathbf{f}$  is the Coriolis parameter,  $p$  is pressure,  $K_m$  is the vertical eddy viscosity,  $\boldsymbol{\omega}$  is vorticity and  $\mathbf{F}_{ds}$  is the wave-induced momentum transfer from waves to ocean due to dissipation of wave energy [*Jenkins, 1987, 1989*],

$$\mathbf{F}_{ds} = -4\pi \int \int f \hat{\mathbf{k}} S_{ds} k e^{2kz} df d\theta, \quad (10)$$

where  $\hat{\mathbf{k}}$  is a unit vector in the direction of  $\mathbf{k}$ . Here  $w$  is vertical velocity,  $\zeta$  is sea surface elevation,  $p_{air}$  is sea level barometric pressure and  $p_g$  is the generalized pressure [*McWilliams et al., 1997*] given by

$$p_g = \frac{1}{2} \rho_o \left( |\mathbf{u} + \mathbf{u}_s|^2 - |\mathbf{u}|^2 \right). \quad (11)$$

[14] The vertical distribution of  $\mathbf{F}_{ds}$  in (10) depends in principle upon the dynamical mechanism by which wave

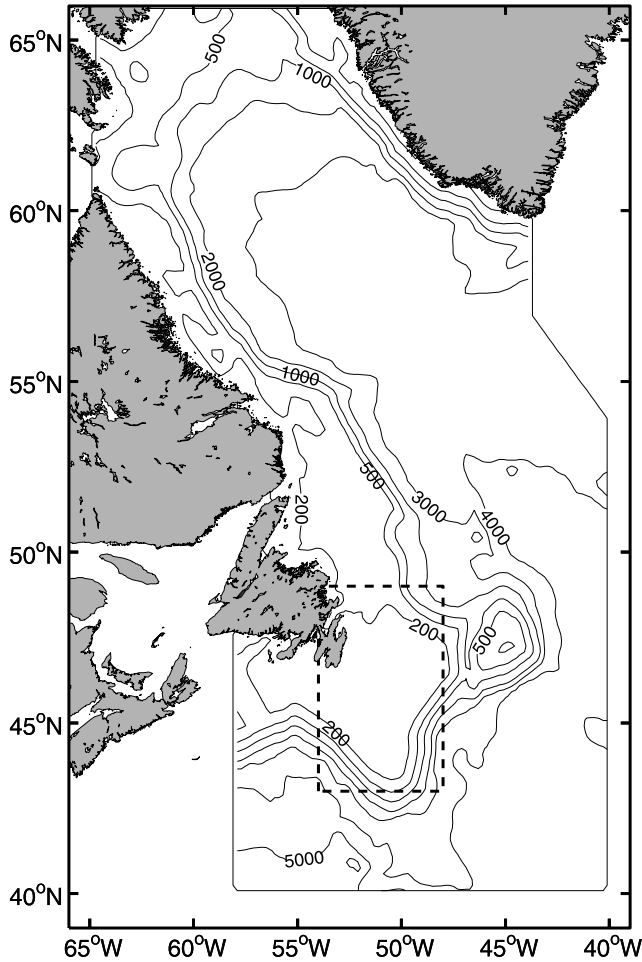


**Figure 1.** POM model domain and bathymetry. The rectangle indicates the study area, encompassing the Grand Banks of Newfoundland.

momentum is converted to momentum of the mean flow. The method we employ follows the philosophy of Hasselmann [1974], who assumed that the dissipation of wave Fourier components was “weak in the mean,” and each component would be damped linearly, with a coefficient possibly depending upon integral properties of the wave spectrum. Since the contribution of a wave component of wave number  $\mathbf{k}$  to the Stokes drift is vertically distributed as  $\exp(2kz)$ , we assume that the transfer of momentum to the mean flow has the same vertical distribution. In the absence of more detailed information from experimental or theoretical studies relevant to operational numerical models, this is the most reasonable formulation to use. In any case, dissipation by wave breaking is a challenging dynamical process, and a quantitatively accurate estimate of the vertical distribution of wave–mean flow momentum transfer due to wave breaking would require the detailed data analysis from laboratory wave tank experiments, field observations and comprehensive time-dependent numerical model investigations. At present, as there is no consensus as to how this should be pursued, this problem is well beyond the scope of this study.

[15] The boundary condition at the sea surface is

$$K_m \frac{\partial \mathbf{u}}{\partial z} \Big|_{z=0} = \frac{1}{\rho_o} (\mathbf{T}_a - \mathbf{T}_{in}), \quad (12)$$

where  $\mathbf{T}_a$  is the wind stress vector and  $\mathbf{T}_{in}$  is the reduction of wind stress due to wave generation. Jenkins [1989] proposed the following form for  $\mathbf{T}_{in}$ :

$$\mathbf{T}_{in} = 2\pi\rho_o \int \int f \hat{\mathbf{k}} S_m d\theta. \quad (13)$$

[16] Close to the sea bottom, the velocity profile follows the law of the wall and the bottom stress is assumed a quadratic function of water velocity with a drag coefficient determined from bottom roughness. The drag coefficient is given by

$$C_D = \left( \frac{\kappa}{\ln H/z_{oa}} \right)^2, \quad (14)$$

where  $\kappa$  is the von Karman constant and  $z_{oa}$  is the apparent bottom. The apparent bottom roughness is the bottom roughness enhanced by wave-current interaction in the presence of waves. It can be several orders of magnitude greater than the conventional bottom roughness [Grant and Madsen, 1979; Mellor, 2002].

## 2.2. Current-Drifter Coupling

[17] The velocity data used in this study are derived from the trajectories of surface drifters. The drifter velocity deviates from the velocity of surface water because wind stress acting on the exposed part of the drifter exerts a force on the drifter that drives it downwind with respect to the surface water in which it resides. The difference between the drifter and surface water velocity, known as leeway, may be estimated from a simple dynamical model of the surface drifter.

[18] The governing equation for the velocity of a surface drifter,  $\mathbf{U}_b$ , can be written as

$$m \left( \frac{d\mathbf{U}_b}{dt} + \mathbf{f} \times \mathbf{U}_b \right) = -mg\nabla\zeta + \mathbf{F}_{air} - \mathbf{F}_{water}, \quad (15)$$

where  $m$  is the mass of the drifter.  $\mathbf{F}_{air}$  and  $\mathbf{F}_{water}$  are the drag forces on above- and below-surface portions of the drifter, respectively. They can be parameterized by quadratic equations,

$$\mathbf{F}_{air} = \frac{1}{2} \rho_a C_{da} A_a |\mathbf{W}| \mathbf{W} \quad (16)$$

$$\mathbf{F}_{water} = \frac{1}{2} \rho_o C_{dw} A_w |\mathbf{U}_b - \mathbf{U}(0)| [\mathbf{U}_b - \mathbf{U}(0)], \quad (17)$$

where  $\mathbf{W}$  is 10-m wind (assuming  $|\mathbf{W}| \gg |\mathbf{U}_b|$ ),  $C_{da}$  and  $C_{dw}$  are the air and water drag coefficients, and  $A_a$  and  $A_w$  are the exposed cross-sectional areas of the drifter above and below the water surface, respectively. The drag

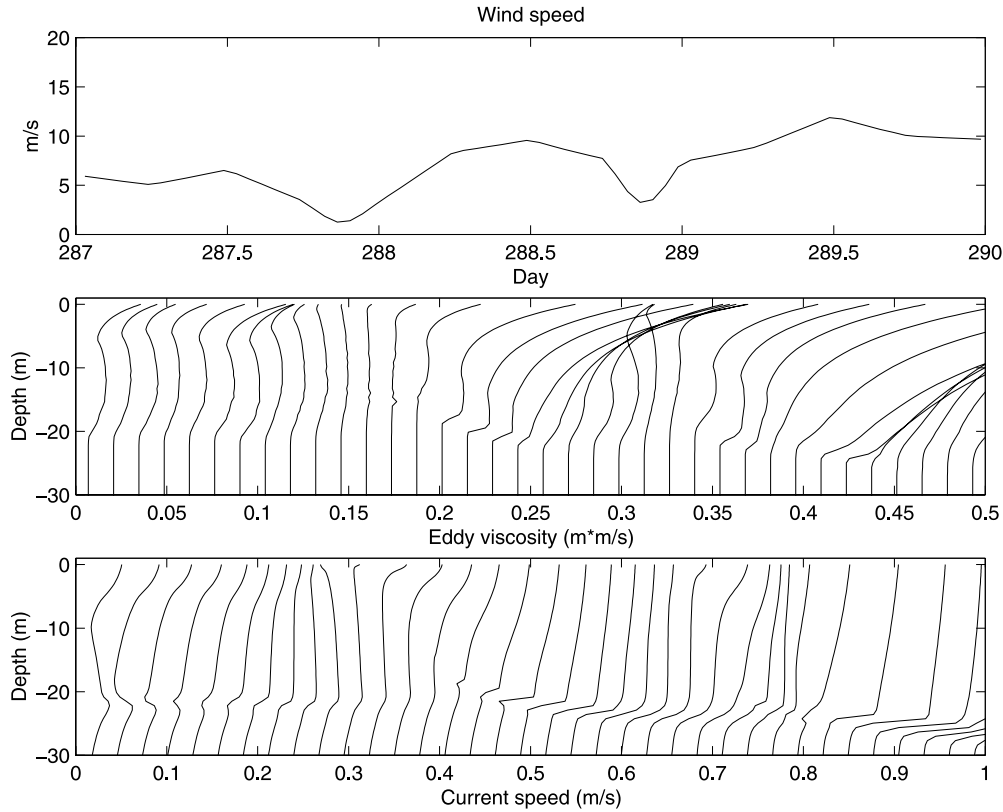


**Figure 2.** (top) Wind speed time series, (middle) vertical profiles of eddy viscosity, and (bottom) current speed computed for days 287–290, 2002 (14–17 October) at 45.4°N, 51.1°W (central Grand Banks) from an 1-D version of POM. The scales of the  $x$  axis of middle and bottom plots are for the first profiles only. Successive profiles are offset by  $0.0138 \text{ m}^2 \text{ s}^{-1}$  in the eddy viscosity and  $0.0278 \text{ m s}^{-1}$  in the speed plots. The positions of the profiles correspond to the times of the top plot.

coefficients depend on the shape of the drifter and the Reynolds numbers based on the relative motions between the drifter and surrounding fluids. They can be estimated from empirical data.  $\mathbf{U}(0)$  is surface velocity defined by (4). In (17), we have assumed that ocean currents do not have a large vertical variation over the submerged portion (also denoted as the draft) of the drifter.

[19]  $\mathbf{U}_b$  can be solved numerically given  $\mathbf{U}(0)$ ,  $\mathbf{W}$  and sea surface elevation from (15)–(17). If the dominant time-scales of the wind greatly exceed the dynamic response time of the drifter and the leeway component of the drift current is small ( $\mathbf{f} \times \mathbf{U}_b \approx F \times \mathbf{U}(0) \approx g \nabla \zeta$ ), the drag forces on the drifter are approximately in equilibrium ( $\mathbf{F}_{\text{air}} \approx \mathbf{F}_{\text{water}}$ ), so that

$$|\mathbf{U}_b - \mathbf{U}(0)| |\mathbf{U}_b - \mathbf{U}(0)| = r^2 |\mathbf{W}| \mathbf{W}, \quad (18)$$

where  $r^2 = (\rho_a C_{da} A_a / \rho_w C_{dw} A_w)$  is a ratio of drag parameters.  $\mathbf{U}_b$  can be solved algebraically from (18) given  $\mathbf{U}(0)$  and  $\mathbf{W}$ .

### 3. Ocean and Wave Models

#### 3.1. Ocean Model

[20] To model the ocean, we use a modified version of the Princeton Ocean Model (POM) implemented for the eastern Canadian seas by Yao *et al.* [2000a]. The model domain (Figure 1) is from 40°N to 66°N and from 40°W to 58°W,

which encompasses the entire study area on the Grand Banks. The boundary conditions and spin-up procedure are the same as those used by Yao *et al.* [2000a] but the vertical levels have been increased from 16 to 23 ( $z/D = 0, 0.0004, 0.0012, 0.0028, 0.006, 0.012, \dots$ ). The water depths,  $D$ , of the Grand Banks vary from 70 to 210 m, which implies that the shallowest depths for velocity range from 1.4 cm to 4.2 cm. The initial temperature-salinity fields represent the October climatology obtained from an objective analysis of archived data at Bedford Institute of Oceanography. The forcing is 6-hourly 10-m winds on a  $1^\circ \times 1^\circ$  grid from the Meteorological Service of Canada (MSC). Surface heat and mass fluxes are set to zero because the primary forcing for surface current is surface wind.

[21] The vertical eddy viscosity in POM takes the form

$$K_m = lqS_m. \quad (19)$$

The vertical profiles of  $l$ , the mixing length, and  $q^2/2$ , the turbulence kinetic energy, are determined by solving the equations for  $q^2$  and  $q^2 l$  in a turbulence closure model embedded in POM. The stability function  $S_m$  depends on vertical shear, buoyancy,  $q$  and  $l$ . In the conventional turbulence closure model,  $l$  is assumed zero and  $q^2$  is proportional  $u_\tau^2$  at the sea surface, where  $u_\tau$  is the water friction velocity. Taking the effects of wave dissipation into consideration, Craig and Banner [1994] and Mellor and

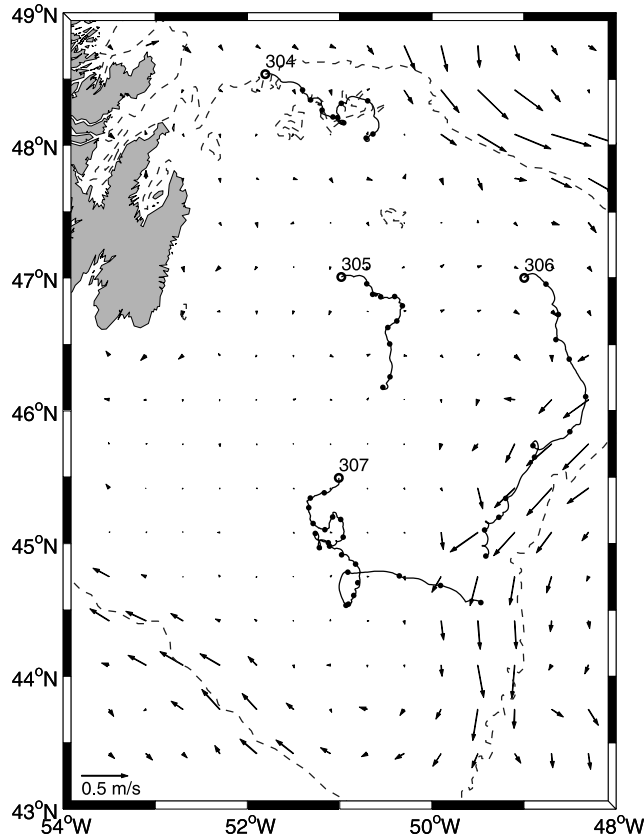


**Figure 3.** Model mean currents (arrows) and drifter trajectories on the Grand Banks. The dots on the trajectories indicate 1-day intervals. The numbers are drifter identification. The open circles indicate the start points of the trajectories. The dashed line is the 2000-m isobath.

Blumberg [2004] proposed new boundary conditions for  $l$  and  $q^2$ . At the surface,  $q^2$  satisfies

$$K_q = \frac{\partial q^2}{\partial z} = 2\alpha_{CB}u_\tau^3, z = 0, \quad (20)$$

where  $K_q$  is the mixing coefficient for turbulence obtained from the turbulence closure model and  $\alpha_{CB}$  is an empirical parameter related to the wave age, the phase speed of waves and the air side friction velocity. The mixing length is given by

$$l(z) = \max[\kappa z_w, l_o(z)] \quad (21)$$

$$z_w = \beta u_\tau^2/g, \quad (22)$$

where  $\beta$  is an empirical parameter, and  $l_o(z)$  is the mixing length obtained by solving the turbulent length scale equation. Here  $\alpha_{CB}$  and  $\beta$  control the vertical profiles of  $K_m$  and hence currents near the surface.

[22] In principle, the values of  $K_m$  obtained from POM should be used to compute the transfer of wave momentum to the mean flow, following (7) and (12). However, any damping of waves due to an assumed eddy viscosity must

be parameterized using an eddy viscosity which is much less than that which acts on the mean flow [Batchelor and Proudman, 1954; Jenkins, 1987, 1989]. In the absence of more detailed information, from experimental studies or elsewhere, we keep the formulation given in (7) and (12).

[23]  $K_m$  is time dependent and, at the surface, varies as the cube of wind speed. To see the relationship among winds, eddy viscosity and current profiles clearly without the influence of advection, land boundary, barotropic flows and other factors, a 1-D version of the ocean model was implemented. Figure 2 shows the profiles of  $K_m$  and current speed for days 287–290. During the periods of low wind speeds, day 287.9 and day 288.9, the profiles of  $K_m$  assume a conventional form, i.e., near zero at the surface and maximum at  $z \sim -10$  m. During high winds, day 288.5 and day 289.5, the maximum  $K_m$  is at the surface.

[24] The surface velocities from a spin-up run of the model without the tidal currents representing the mean surface currents are shown in Figure 3. The most prominent feature of the mean current field is the strong Labrador Current along the eastern shelf edge of the Grand Banks. The core of the Labrador Current is at the 500- to 1000-m isobaths [Tang et al., 1996]. Currents in the interior of the Grand Banks are relatively weak.

### 3.2. Wave Model

[25] To model waves, we use Wavewatch III (hereafter WW3), version 2.22. WW3 is a discrete spectral phase-averaged model [Tolman, 2002], which resolves the directional spectrum at each model grid point in terms of wave number-direction bands. Wave generation and development is determined numerically by solving the spectral wave action conservation equation, which is related to the spectral energy balance equation (6) by the relation

$$E = N \sigma. \quad (23)$$

$N(t, x, y, f, \theta)$  is the wave action spectrum, and  $t$  is time and  $\sigma$  is the intrinsic frequency which is related to wave number  $k$  by the dispersion relation  $\sigma^2 = gk$  and  $2\pi f\sigma + \mathbf{k} \cdot \mathbf{u}$ . WW3 has been extensively validated by NCEP over the last several years. In this study, we focus on the impact of waves on wind-driven currents on short timescales, rather than the impact of relatively strong permanent currents such as the Gulf Stream on waves. Therefore we neglect the effects of currents in (6).

[26] Two formulations for  $S_{in}$  and  $S_{ds}$  are considered in this study: the conventional WAM cycle 3 parameterizations for  $S_{in}$  and  $S_{ds}$  [WAMDI Group, 1988], as the baseline experiment (Section 5), and the more recent  $S_{in}$ ,  $S_{ds}$  parameterizations of Tolman and Chalikov [1996] and Tolman [2002] in WW3 (hereafter denoted the ‘WW3’ formulation) in the sensitivity experiments (section 7). The latter parameterizations are motivated by theoretical and experimental considerations related to wave-induced drag, and wave feedbacks on the atmospheric boundary layer, and tend to result in a slight overall reductions in wave growth, compared to earlier WAM formulations. However, in terms of forecast skill, for global ocean studies and comparisons with in situ data, these  $S_{in}$  and  $S_{ds}$  parameterizations represent the overall state-of-the-art.

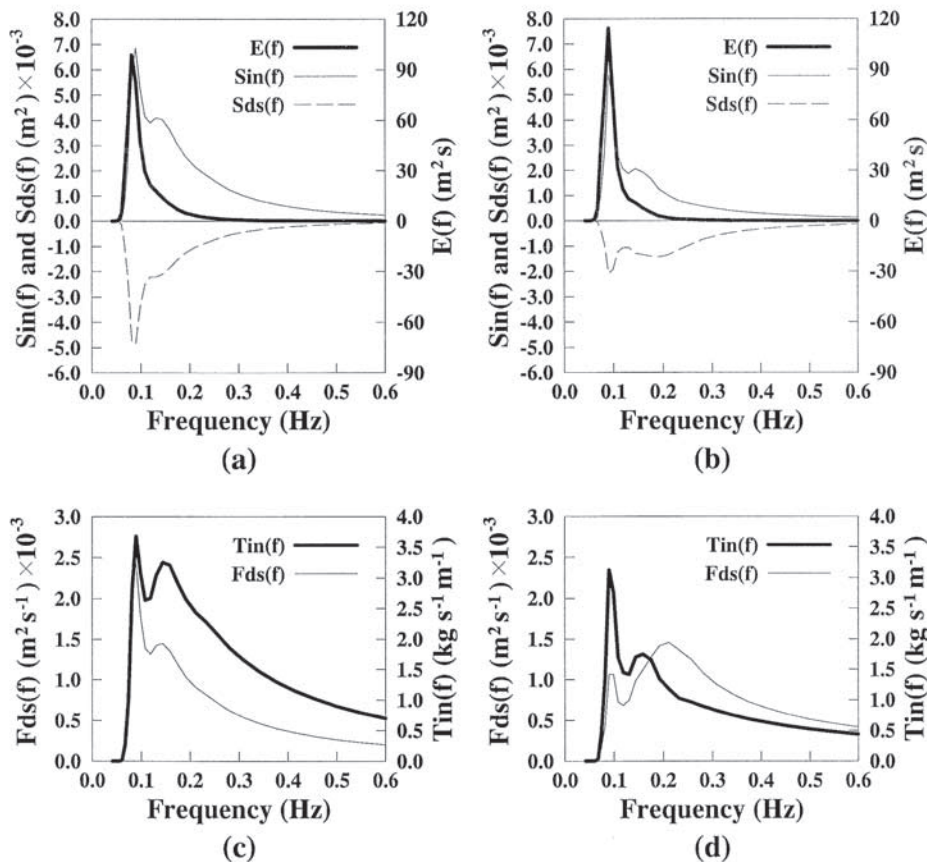


**Figure 4.** Variation of source terms  $S_{in}$  and  $S_{ds}$  as a function of frequency  $f$  at the peak of the storm (maximum waves), 12 UTC on 29 October for (a) WAM cycle 3 versions of terms  $S_{in}$  and  $S_{ds}$  and (b) versions of  $S_{in}$  and  $S_{ds}$  from *Tolman and Chalikov* [1996]. Corresponding variations for (c) the integrand of equation (10) for  $F_{ds}$  (denoted here as  $F_{ds}(f)$ ) and (d) the integrand of equation (13) for  $T_{in}$  (denoted as  $T_{in}(f)$ ), with  $\theta$  wave direction and ( $z$ ) depth dependence integrated out. Units for wind input and wave dissipation are  $\text{m}^2/\text{Hz}$ , and for wave spectra energy  $E(f)$ ,  $\text{m}^2/\text{s}/\text{Hz}$ .

[27] In terms of wave momentum and the flux of momentum from wind to waves and from waves to currents, expressions for  $F_{ds}$  and  $T_{in}$  include factors of  $f$ , which as well as factors of  $S_{ds}$  and  $S_{in}$ , respectively. The  $S_{in}$  and  $S_{ds}$  formulations have their maximal and minimal values, respectively, in the general neighborhood of the spectral peak  $f_p$ , as shown by Figures 4a and 4b. The  $f$ -dependent factors modulate the contributions to  $F_{ds}$  and  $T_{in}$  from  $S_{ds}$  and  $S_{in}$  terms, so that the integrands for  $F_{ds}$  and  $T_{in}$  (when integrated over the water column) have maxima that occur at slightly high  $f$  values than the maximal variations of  $S_{in}$  and  $S_{ds}$ . This is shown in Figures 4c and 4d.

[28] It is evident from Figures 4a and 4b that contributions to the wave-induced currents from the formulations for  $S_{in}$  and  $S_{ds}$  from *Tolman and Chalikov* [1996] are different, compared to contributions from the WAM cycle 3 versions for  $S_{in}$  and  $S_{ds}$ . This difference in contributions has impact on the impacts of  $F_{ds}$  and  $T_{in}$ . Moreover, the way in which these wave models treat the high-frequency tail of the wave spectrum is not discussed here, because in both the WW3 and WAM versions used here, the wave spectrum is explicitly computed up to  $3f_p$  and follows the same  $f^{-4}$

variation, beyond which the spectral tail is assumed to follow an  $f^{-5}$  variation. This variation is consistent with recent studies by *Resio et al.* [2004], suggesting an  $f^{-4}$  equilibrium range over the approximate range of  $2f_p-4f_p$  and a dissipative  $f^{-5}$  region beyond this domain.

## 4. Wind and Surface Drifter Data

### 4.1. Wind Fields

[29] During the autumn, cyclones typically pass over the Grand Banks and eastern Canada, following a southwest-to-northeast storm track. These storms include extratropical hurricanes and Nor'easters. Individual storms are interspersed with relatively quiet periods. The typical timescale for a storm event to pass a given location is about 2–4 days, although shorter and longer events do occur. During the study period, 8–31 October 2002, the storm of 27–31 October constitutes one of the more intense meteorological systems passing over this region. Minimum sea level pressure reached 978 hPa and maximum winds of  $26 \text{ m s}^{-1}$  were experienced at 1200 UTC on 31 October over an extensive area of the Grand Banks and southern Labrador Sea. As the storm

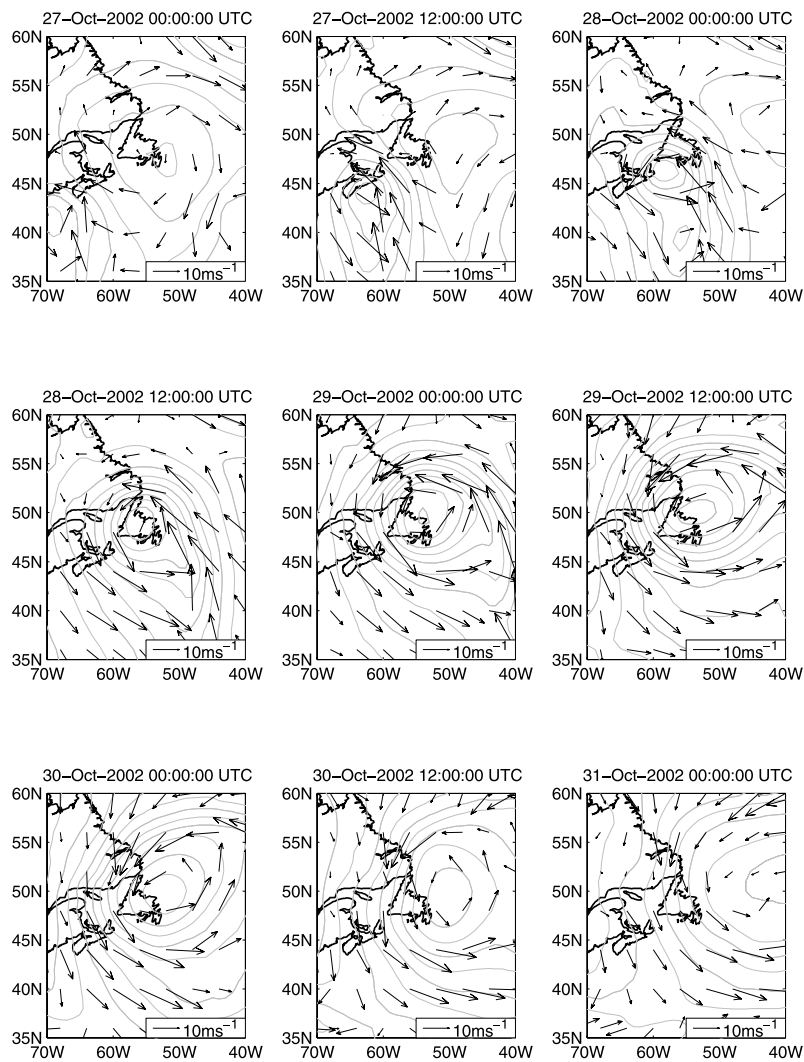


**Figure 5.** Sea level pressure and wind vectors for the 27–31 October storm passing over eastern Canada and Grand Banks, as provided by MSC. Maximum winds reached  $26 \text{ m s}^{-1}$  at 1200 UTC on 31 October.

developed and intensified, it propagated toward the northeast over the Grand Banks and southern Labrador Sea and thereafter weakened, as it moved toward its lysis region (Figure 5).

**4.2. Surface Drifter Data**

[30] Four surface drifters were deployed on the Grand Banks in October 2002 by Canadian Coast Guard (Figure 3 and Table 1). The duration of their trajectories varies from 11 to 23 days. Toward the end of the study period, only drifter 307 remained on the Grand Banks. The drifter data

were transmitted to shore via satellites at a rate of 3 to 12 positions per hour. The raw data were despiked, fitted with a second-order polynomial in a moving window of 4 hours and decimated to 1-hour intervals [Dunlap *et al.*, 2004]. Drifters 304, 305 and 307 were on the Grand Banks

**Table 1.** Information on Drifter Data

| Drifter ID | Start, UTC      | End, UTC         | Duration, days |
|------------|-----------------|------------------|----------------|
| 304        | 1200, 8 October | 1200, 18 October | 11             |
| 305        | 1200, 8 October | 1200, 18 October | 11             |
| 306        | 1200, 8 October | 2100, 20 October | 13             |
| 307        | 1200, 9 October | 1200, 31 October | 23             |

**Table 2.** Parameter Values in the Baseline Experiments

| Model         | Symbol        | Value in Baseline Runs | Parameters  |
|---------------|---------------|------------------------|---|
| Ocean model   | $\alpha_{CB}$ | 150                    | $q^2$ boundary condition parameter (equation (20))              |
|               | $\beta$       | $4 \times 10^5$        | mixing length parameter (equation (22))                         |
|               | $z_o$         | 0.01 m                 | bottom roughness  |
|               | $z_{oa}$      | 0.1 m                  | apparent bottom roughness                                       |
| Drifter model | $r^2$         | $0.18 \times 10^{-4}$  | drag parameter ratio (equation (18))                            |
| Wave model    | WAM           |                        | $S_{in}$ and $S_{ds}$ parameterizations from WAMDI Group [1988] |

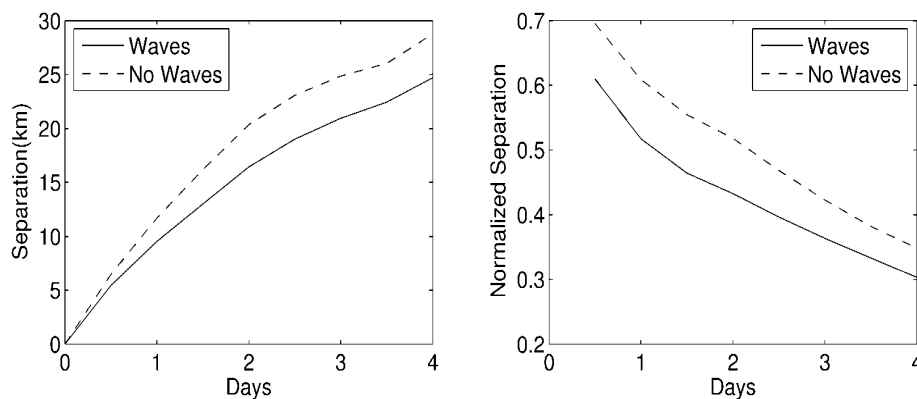


**Figure 6.** (left) Mean separation and (right) normalized separation as a function of time from two model experiments: experiment (a), dashed lines (no wave); and experiment (b), solid lines (full wave effects).

at all times. The mean water depth of the Grand Banks is 80 m, and the mean currents are weak and in the southward direction. Drifter 306 moved along the shelf edge following the Labrador Current most of the time (Figure 3).

## 5. Comparison of Model Simulations With Data

[31] We compare the modeled and observed surface velocities and trajectories. Our aim is to determine whether the inclusion of wave effects in the ocean model could improve the predictions of surface currents on a timescale of several days. Waves effects are investigated from three baseline model experiments: In experiment (a), “no waves,” the quantities  $\mathbf{u}_s$ ,  $F_{ds}$  and  $T_{in}$  in (4), (7) and (12) are set to zero and the apparent bottom roughness  $z_{ao}$  in (14) is replaced by the bottom roughness  $z_o$ ; in experiment (b), “full wave effects,” the velocity  $\mathbf{u}$  is computed from the full set of equations, (7)–(14) and (18), plus the Stokes drift and the tidal currents; and in experiment (c), “Stokes drift only and no air-wave-current momentum transfer,” we set  $F_{ds}$  and  $T_{in}$  to zero but keep the Coriolis term associated with the Stokes drift in (7) and add the Stokes drift and the tidal currents to  $\mathbf{u}$ .

[32] Recognizing that there are uncertainties in the parameters for all three models (waves, ocean and drifter), a standard set of parameter values within their allowable ranges is adopted (Table 2) in order to generate reasonable simulations of the observed drift trajectories. We then deduce the effects of waves on the drift from an analysis of the results of the three experiments. In the following sections, all model currents are vertically averaged over the top 1 m in order to avoid bias associated with the variable vertical grid size.

### 5.1. Separation as a Function of Time Intervals

[33] The drifter trajectories were broken up into segments of varying time intervals. For each segment, the separation between the end points of the modeled and observed trajectories was calculated. By including the wave effects, the mean separation decreases from 12 km to 9.5 km at day 1, and from 20.5 km to 17 km at day 2 (Figure 6, left). These results represent an improvement of 21% at day 1 and 17% at day 2 from the no-wave to with-wave simulations.

[34] To remove the influence of mean currents on the statistics, so that the results can be compared to observations from other regions, separations normalized by the length of the observed trajectories were computed (Figure 6, right). The relative errors decrease with time. A possible explanation for the decreasing relative errors is that short-period motions such as inertial oscillation and diffusion are not well simulated by the model. A similar behavior was also found in wind-driven ice movement [Yao *et al.*, 2000b]. The model simulations with the wave effects reduce the relative error by 0.1 at day 1, and by 0.06 at day 3.

### 5.2. Vector Regression Analysis

[35] To assess the wave effects on surface velocity quantitatively, a vector regression analysis was carried

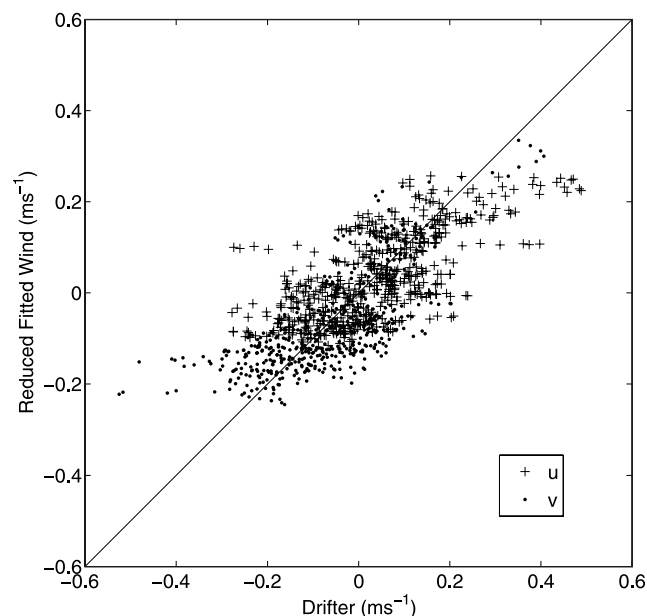


**Figure 7.** Scatterplot of the  $u$  and  $v$  components of scaled winds (wind speed times speed ratio and wind direction rotated by turning angle) versus modeled surface currents for drifter 307.

**Table 3.** Speed ratio, Turning Angle, and Correlation Coefficient for the Three Drifters on the Grand Banks (304, 305, 307) From the Vector Regression Analysis<sup>a</sup>

|                         | Observation | Model                     |                                     |
|-------------------------|-------------|---------------------------|-------------------------------------|
|                         |             | Experiment (a)<br>No Wave | Experiment (b) With<br>Wave Effects |
| Speed ratio, %          | 2.06        | 1.54                      | 2.07                                |
| Turning angle, deg      | 30.2        | 58.0                      | 33.9                                |
| Correlation coefficient | 0.97        | 0.71                      | 0.99                                |

<sup>a</sup>The range of correlation coefficients is from 0 to 2 [Crosby *et al.*, 1993].

out. The drifter velocity is assumed to be the sum of a wind-driven component and a non-wind-driven component. The former is taken to be wind velocity reduced by a factor  $R$  and rotated by an angle  $\phi$ . In complex notation, the relation between the drifter velocity,  $U_b$ , and the wind,  $W$ , can be written as

$$U_b = R \cdot W \exp(i\phi) + U_o, \quad (24)$$

where  $U_o$  is the velocity of non-wind-driven motion. A negative  $\phi$  means the drifter direction is rotated clockwise from the wind direction. We denote  $R$  as the speed ratio and  $-\phi$  as the turning angle. Given time series  $U_b$  and  $W$ , (24) can be used to determine optimal values for  $R$ ,  $\phi$  and  $U_o$ , from a least squares fit. In this analysis,  $U_b$  are hourly model or drifter data and  $W$  is hourly wind interpolated to the drifter positions.

[36] The vector regression analysis was carried out for each drifter and the three baseline experiments separately. Figure 7 is a sample scatterplot of east and north components of the scaled and rotated winds computed from (24) versus the observed surface velocities for drifter 307. The scattering of the data points can be caused by motions that are not directly related to wind, such as tidal currents and inertial currents. For each assembly of vector pairs such as those shown in Figure 7, a correlation coefficient was computed. We use the method of Crosby *et al.* [1993] to compute the correlation coefficients,  $\rho$ , between two vector time series,  $w_1$  and  $w_2$ ,

$$\rho^2 = \text{Tr}[(\Sigma_{11})^{-1}\Sigma_{12}(\Sigma_{22})^{-1}\Sigma_{21}],$$

where  $\Sigma_{ii}$  is the covariance matrix of  $w_i$ , and  $\Sigma_{ij}$  is the cross-covariance matrix of  $w_1$  and  $w_2$ . In this formulation, the range of  $\rho$  is from 0 to 2.

[37] The correlation coefficients for drifter 306 are low (0.44 for the model and 0.47 for the data). This implies that the relationship between wind and surface current is not linear. Factors other than wind, such as pressure gradient and shelf waves, can be more important in driving the currents. A large portion of the trajectory of drifter 306 is in the Labrador Current (Figure 2), where pressure gradients are enhanced and shelf waves generated upstream propagating to the Grand Banks have maximum magnitude [Tang *et al.*, 1998]. Both the pressure gradients and shelf waves can be generated by wind but they are not directly correlated to the wind vectors, as is the case for Ekman currents in an open ocean.

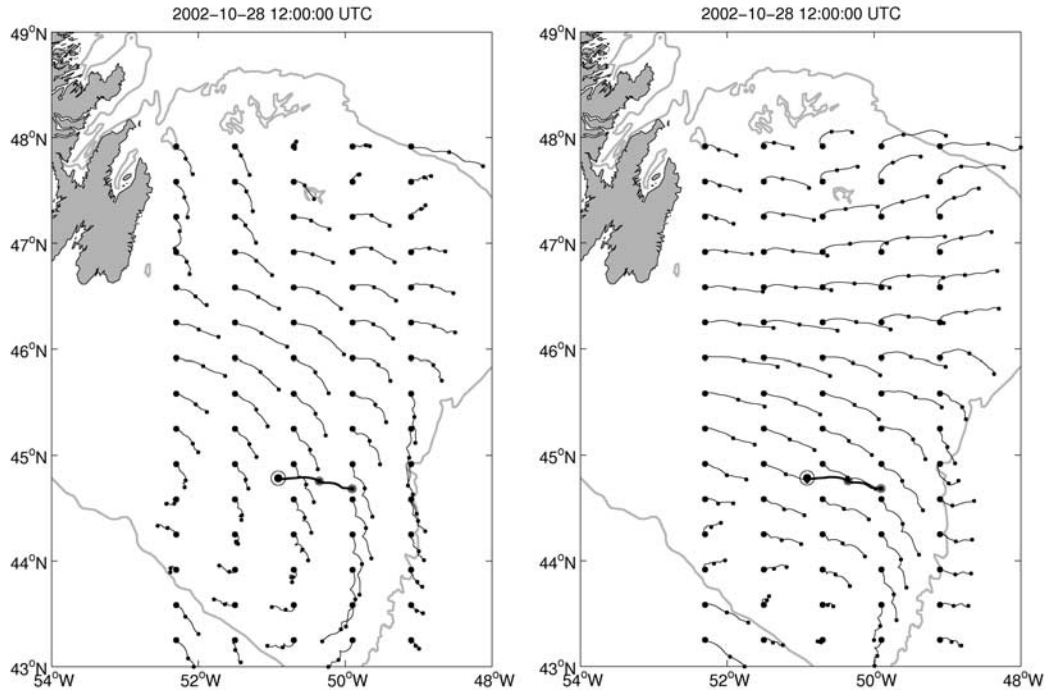


**Figure 8.** Two-day model trajectories (28 October, UTC 1200, to 30 October, UTC 1200) (left) without and (right) with the wave effects from the model (thin lines). The thick lines are the observed trajectory in the same period. The solid circles (model) and the open circles (observation) denote the start point.

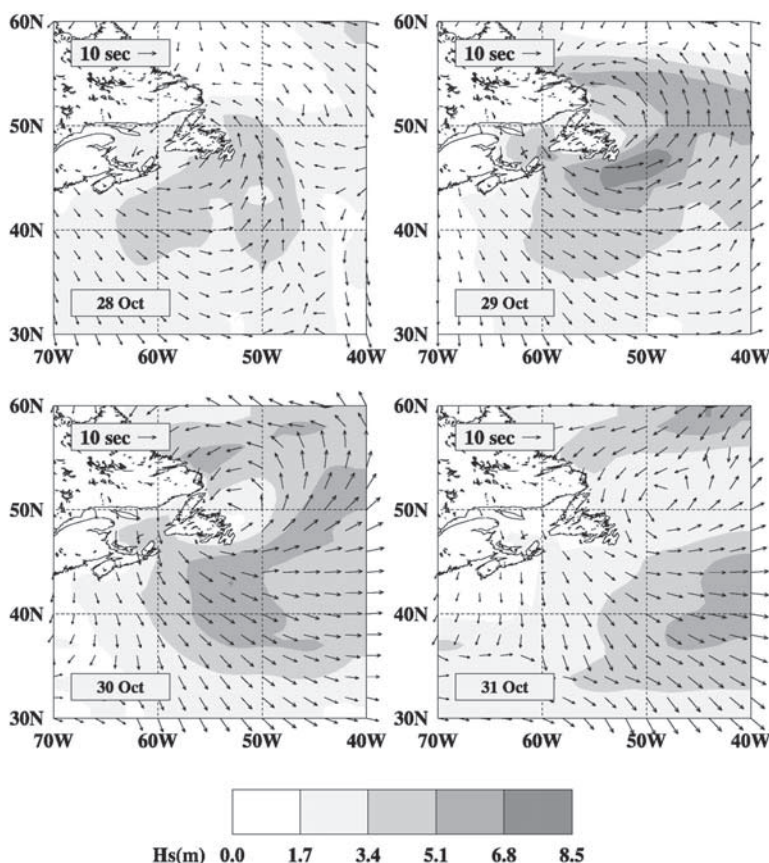


**Figure 9.** Ocean wave height (shades) and direction and period (arrows) for 28, 29, and 30 October, UTC 1200.

[38] The correlation coefficients for the three drifters on the Grand Banks (304, 305, 307) range from 0.61 to 1.27. These relatively large values mean that the relationship between the winds and surface velocities is approximately linear. The results of the regression analysis shown in Table 3 are the averages of the three drifters weighted by the correlation coefficients. On average, the observed drifter speeds are 2.06% of the wind speeds and the directions are  $30^\circ$  clockwise from the wind directions. The simulation with wave-current coupling, experiment (b), gives a mean speed ratio of 2.07% and a mean turning angle of  $34^\circ$ . These results compare well with the observations. The simulation without waves, experiment (a), underpredicts the speed ratio by 0.52% and overpredicts the turning angle by  $28^\circ$ . The increase in surface speed from experiment (a) to experiment (b) is 35%.

[39] The mean correlation coefficient is moderate (0.97 out of a possible 2.0) for the observed drifter velocity indicating that a portion of the surface currents is not directly correlated to winds. The non-wind-driven currents can include tidal currents, mesoscale eddies and random diffusion. The correlation coefficient from experiment (b) is 0.99, which is significantly larger than the correlation coefficient from experiment (a), 0.71.

[40] In the presence of a wavefield, the wind stress available for current generation is reduced by an amount proportional to  $S_{in}$  (equation (12)). However, this reduction

in wind stress is partially compensated by the wave momentum flux into the ocean which causes an increase in current speed. The net effect of the wind-wave-current momentum transfer is to reduce the current speed. The magnitude of the reduction can be determined from a regression analysis between the surface velocities from experiments (b) and (c). The analysis for the three drifters gives speed ratios ranging from 95.8% (drifter 307) to 98.7% (drifter 304), which means the wind-wave-current momentum transfer reduces the surface current speeds by approximately 1–4%. The turning angles are insignificant. These results indicate that the wave effect is dominated by the Stokes drift.

## 6. Stokes Drift

[41] To gain a better understanding of how the Stokes drift changes surface currents, we examine the current and wavefields during a period of strong winds. Figure 8 shows 2-day trajectories from the model and drifter 307 starting at 1200 UTC, 28 October (the only drifter still transmitting data at this time). This period is the middle of the storm mentioned in the previous section. When waves are excluded (Figure 8a), we see that the model trajectories deviate significantly from the observed drifter trajectory (thick line). However, waves develop and impact on this current field following the overall development, intensifi-

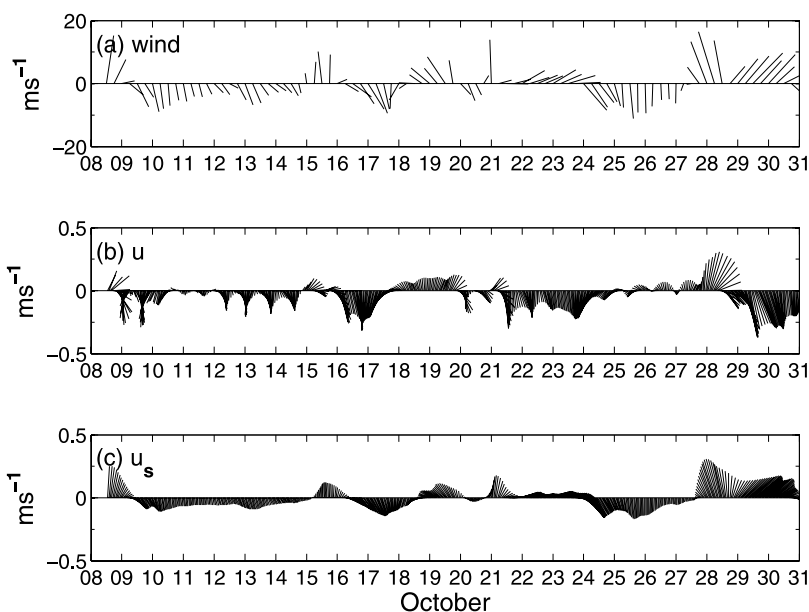


**Figure 10.** Time series at 46°N, 50°W of (a) winds, (b)  $u$  from POM, and (c) the Stokes drift,  $u_s$ , computed from (5) using wave spectra from WW3 with terms  $S_{in}$  and  $S_{ds}$  from WAM cycle 3.

cation and weakening of storms, as they propagate across the Grand Banks and Labrador Sea (Figure 5). The Stokes drift has a pattern that is similar to the wavefields (Figure 9). The Stokes drift moves the water toward the wind and dominant wave directions. This is shown in the change in current directions due to the wave effects in Figure 8b.

[42] The relationship between winds and the Stokes drift can be examined from time series plots of winds,  $u$ , and  $u_s$ , at a fixed location, 46°N, 50°W (Figure 10). The Stokes drift is linearly related to the wind velocities approximately. A consequence of the relationship is that the total currents (4) are closer to the wind directions than the model currents without the wave effects, shown in Figure 8a. The mean

Stokes speed averaged over the study area varies from 0.5% at low wind speeds to 2.1% at high wind speeds with a mean of 1.48%. This is compatible with the observed 1.25% “bubble-weighted” value, which is averaged over the top few meters, as reported by *Smith* [2006].

[43] Integrating (5) over  $\theta$ , we obtained the Stokes drift as a function of frequency and distance below the ocean surface (Figure 11). The contributions to the Stokes drift are maximal in the peak region of the wave spectrum (Figure 4a). The Stokes drift attenuates vertically as  $\exp(2kz)$ . The attenuation scale,  $L = (2k)^{-1}$ , decreases with frequency as  $\sim f^{-2}$ . At 0.09 Hz (the peak frequency in Figure 11) and 0.2 Hz (20% of the peak value),  $L$  is found

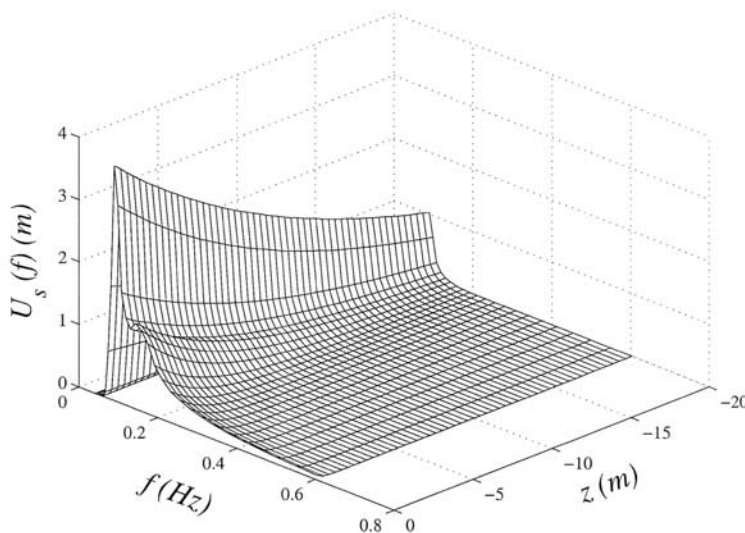


**Figure 11.** Stokes drift as a function of frequency and distance below the ocean surface from (5) using terms  $S_{in}$  and  $S_{ds}$  from WAM cycle 3 at 1200 UTC on 29 October when the storm waves were maximal.

**Table 4.** Comparison of Speed Ratio and Turning Angle Between the Baseline and Sensitivity Experiments<sup>a</sup>

| Parameter        | Value                | Speed Ratio, % | Turning Angle, deg | Correlation Coefficient |
|------------------|----------------------|----------------|--------------------|-------------------------|
| Base set         | Table 2              | 2.07           | 33.9               | 0.99                    |
| $\alpha_{CD}$    | 50                   | 2.14           | 33.9               | 1.02                    |
| $\beta$          | $2 \times 10^5$      | 2.32           | 33.6               | 1.10                    |
| $z_{oa}$         | 0.5 m                | 2.06           | 33.7               | 1.00                    |
|                  | 0.01 m               | 2.11           | 34.9               | 1.00                    |
| $r^2$            | $0.4 \times 10^{-4}$ | 2.13           | 32.3               | 1.00                    |
| $S_{in}, S_{ds}$ | WW3                  | 1.99           | 35.9               | 0.94                    |

<sup>a</sup>Turning angle is clockwise from the wind direction in degree. The values shown are the means of drifters 304, 305, and 307 weighted by the correlation coefficients. The range of correlation coefficient is 0 to 2.

to be 15.3 m and 3.1 m, respectively. These scales indicate that the Stokes drift can have a significant impact on bottom currents in shallow waters with depths less than 20 m. For the Grand Banks where the mean water depth is 80 m, the wave influence does not reach the bottom.

## 7. Sensitivity Experiments and Errors

[44] The ocean, waves and drifter models have several adjustable parameters including  $\alpha_{CB}$  and  $\beta$  in the eddy viscosity, apparent bottom roughness  $z_{ao}$ , drag parameter ratio  $r$  and the wind input  $S_{in}$  and wave dissipation  $S_{ds}$  terms. To assess the sensitivity of the overall coupled model to these parameters, we conducted six additional model experiments (Table 4) each with one parameter value different from the baseline experiments (Table 2). The results indicate that in general the changes in the parameter values have minimal effect on the turning angle, and the range of the speed ratio in Table 4 is much smaller than the difference between experiments (a) and (b) in the baseline experiments (Table 3).

[45] Here  $\alpha_{CB}$  and  $\beta$  control the profile of the eddy viscosity,  $K_m$ , near the surface. From the observations of Terray *et al.* [1996], Mellor and Blumberg [2004] suggests that  $\alpha_{CB}$  is in the range 57–146;  $\beta$  is related to the phase velocity and friction velocity of wavefields. Stacey [1999] used a range of values for  $\beta$  to fit near surface current data in the Knight Inlet (51°N, 126°W) and found the upper bound to be  $8 \times 10^5$ . Table 4 shows that a decrease in  $\alpha_{CB}$  or  $\beta$  leads to an increase in surface currents. In the ranges of  $\alpha_{CB}$  and  $\beta$  considered here,  $\beta$  has a greater impact on surface current than  $\alpha_{CB}$ . A decrease of  $\beta$  by 50% results in an increase of surface current by 12%. The increase is closely related to the profile of eddy viscosity near the surface. Figure 12 shows the mean eddy viscosity for  $\beta = 4 \times 10^5$  and  $2 \times 10^5$  at low (Figure 12, left) and high wind speeds (Figure 12, right) computed from a 1-D version of POM. At low wind speeds, the profiles below 3 m have the conventional form of a maximum in the mixed layer. The increase near the surface is a consequence of wave dissipation implemented in the Craig-Banner boundary condition (20). At high wind speeds,  $K_m$  decreases monotonically with depth. The turbulence closure model in POM gives an eddy viscosity which varies with  $\beta$  and wind speed as  $\beta W^3$  at the surface. A 50% decrease in  $\beta$  results in a decrease of the surface eddy viscosity by the same amount.

[46] In the presence of waves, the apparent bottom roughness,  $z_{ao}$ , is a function of wave orbital velocity and friction velocity near the bottom. Its value can be one or more orders of magnitude larger than the actual roughness [Grant and Madsen, 1979; Mellor, 2002]. For the Grand Banks, the apparent bottom roughness is estimated to be 5 to 100 times the actual roughness. Table 4 shows that changing  $z_{ao}$  from 0.1 m to 0.5 m decreases the surface current slightly. A decrease from 0.1 m to the conventional roughness without wave effects, 0.01 m, results in an increase of the speed ratio by 0.04%. For accurate modeling of currents in shallow oceans, the effect of waves on bottom roughness should not be ignored.

[47] The “leeway” component of the surface drifter motion may be derived from the equilibrium force balance on the drifter following (18), by resolving the buoy and current velocities into downwind and crosswind components. The crosswind balance indicates that the buoy and current components are equal, whereas the downwind balance implies that,

$$U_{leeway} = [U_b - U(0)]_{downwind} = rW. \quad (25)$$

Equation (25) states that the leeway is simply the wind speed scaled by  $r$ . The estimated value of  $r^2$  (Table 2) is based on the frontal areas (in air and water) of the surface drifters and the drag coefficients in air and water. This assumes the Reynolds number, Re, satisfies the condition  $10^4 < \text{Re} < 2 \times 10^5$ , and that  $C_{da}$  and  $C_{dw}$  are of the order  $O(1)$  [Gray, 1972], where Re is based on the relative velocity between fluid and object. Smith [1992] conducted a series of tests using experimental and commercially available buoys in the Bedford Basin, near Halifax, N.S., and found that the observed buoy speeds relative to the surface currents were consistent with the above relationship [Smith, 1992; Smith *et al.*, 1999].

[48] Errors in the drag parameter ratio,  $r^2$ , result mostly from the area ratio, due to the unknown actual configuration of the drifter and drogues in situ, and the air and water drag coefficients. Using a 30% maximum error in the area ratio (and thus  $r^2$ ) would lead to a 14% error in the leeway component, whose maximum is estimated to be roughly  $20 \text{ cm s}^{-1}$ . Hence the errors in the leeway estimates are expected to be less than  $\pm 3 \text{ cm s}^{-1}$ .

[49] An increase from  $0.18 \times 10^{-4}$  to  $0.4 \times 10^{-4}$  in  $r^2$  leads to an increase of the speed ratio by 0.06% (Table 4). This is smaller than the increase predicted by (25). The small increase from the model simulation is due to the fact that only the downwind component of surface velocity will be enhanced by leeway. If the downwind component is negative (wind and drifter in opposite directions), drifter speed can be smaller than the surface current speed. Equation (25) represents the maximum leeway.

[50] The wind input  $S_{in}$  and dissipation  $S_{ds}$  parameterizations used in Table 4 are the formulations of Tolman and Chalikov [1996] and Tolman [2002], as noted in section 3.2. These  $S_{in}$ ,  $S_{ds}$  parameterizations result in a reduction in surface speed by about 4%, relative to the baseline experiment using the WAM cycle 3 parameterizations for  $S_{in}$  and  $S_{ds}$ , and a slight modification in the turning angle. This result is consistent with the tendency for the former to give

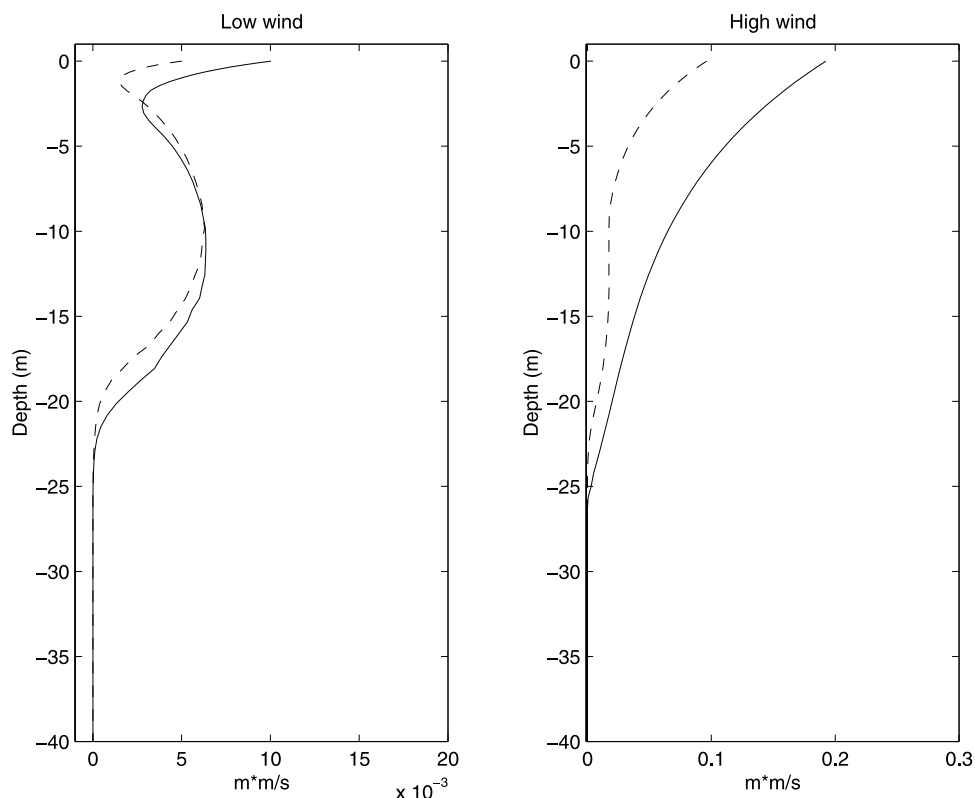


**Figure 12.** Mean eddy viscosity profiles from the 1-D version of POM. (left) Wind speeds less than  $5 \text{ m s}^{-1}$ . (right) Wind speeds greater than  $10 \text{ m s}^{-1}$ . The solid lines are for  $\beta = 4 \times 10^5$  in the baseline experiments. The dash lines are for  $\beta = 2 \times 10^5$  in the sensitivity experiment.

slight overall reductions in wave growth, compared to earlier WAM cycle 3 formulations.

## 8. Summary and Concluding Remarks

[51] We investigated the effects of waves on surface currents using a coupled wave-ocean-drifter model, based on Jenkins' formulation and surface velocity data derived from surface drifters. There are two major wave effects in Jenkins' theory, the Stokes drift and air-wave-current momentum transfers. The Stokes drift can increase surface current speed significantly, by 35%, and turn the currents toward the wind direction. The momentum transfers can reduce the surface speed by a few percent and have minimal effect on the directions. In comparison, the Stokes drift is by far the most important factor of the wave effect. On average, the observed drifter speeds are 2.06% (speed ratio) of wind speeds and the directions are  $30^\circ$  clockwise from wind direction. Without wave-current coupling, the model underpredicts the speed ratio by 0.52% and overpredicts the turning angle by  $28^\circ$ . On the Grand Banks, the winds and surface velocities are approximately linearly correlated and wave effects improve the correlation coefficients significantly, from 0.71 without waves, to 0.99 with waves (the range of vector correlation coefficient is 0 to 2, following Crosby *et al.* [1993]). In the Labrador Current, winds and surface currents are not linearly correlated owing to the influence of shelf waves and other factors. The model performance can be measured by the separation between the modeled and drifter trajectories. Improvement in the

model performance, comparing the no-waves experiment to the experiment with waves, is approximately 21% at day 1 and 17% at day 2.

[52] The sensitivities of the model currents to eddy coefficients, bottom friction, air drag and wind input and dissipation parameterizations are investigated. The speed ratio is most sensitive to the surface eddy coefficient, moderately sensitive to air drag and wind input and dissipation parameterizations for waves, and least sensitive to bottom friction. A 50% decrease in the surface eddy coefficient will increase surface current speeds by 12%. The impact of wave dynamics source term parameterizations should not be ignored, varying by about 4% in surface current speeds, comparing the results from WAM cycle 3  $S_{in}$  and  $S_{ds}$  parameterizations, to those of WW3 parameterizations. The turning angle is not sensitive to any parameter.

[53] There are other uncertainties that influence estimates of surface currents, such as errors in wind data and model boundary conditions. However, such errors are unrelated to wave-ocean interactions but will affect the accuracy of the simulations. They will be dealt with in future investigations.

[54] This study tests the theory of wave-current interaction using an operational wave forecast model, and a realistic 3-D circulation model with time and depth varying eddy viscosity and comparing the model simulations to surface drifter data. To improve the statistics and obtain optimal values of the model parameters, more surface current measurements in different geographic locations are required. Other than surface drifters, high-quality surface current data can be obtained from sequential satellite images

[e.g., Liu et al., 2006] and high-frequency radars [e.g., Paduan et al., 2004; Ullman and Codiga, 2004; Bassin et al., 2005]. These data can provide information about the horizontal structure of surface current fields and are excellent data sources for studying surface currents.

[55] **Acknowledgments.** The research has been supported by the Canadian Panel on Energy Research and Development, the Canadian Coast Guard NIF, the Canada Foundation for Atmospheric and Climate Studies CFCAS, and SURA, the Southeast University Research Association through SCOOP, the SURA Coastal Ocean Observing Program. A. D. Jenkins has received support from the Research Council of Norway under projects 155923/700 and 175763/V30, and the Aurora Programme for French-Norwegian Research Collaboration. We thank Jean Maillette, Katherine MacIntyre, and Ron Dawson of the Canadian Coast Guard for deploying the surface drifters used in this study and making the data available to us. Ewa Dunlap and Yongsheng Wu gave helpful suggestions to improve the manuscript.

## References

- Andrews, D. G., and M. E. McIntyre (1978a), An exact theory of nonlinear waves on a Lagrangian-mean flow, *J. Fluid Mech.*, **89**, 609–646.
- Andrews, D. G., and M. E. McIntyre (1978b), On wave-action and its relatives, *J. Fluid Mech.*, **89**, 647–664.
- Ardhuin, F., B. Chapron, and T. Elfhøj (2003), Waves and the air-sea momentum budget, implications for ocean circulation modelling, *J. Phys. Oceanogr.*, **34**, 1741–1755.
- Bassin, C. J., L. Washburn, M. Brzezinski, and E. McPhee-Shaw (2005), Sub-mesoscale coastal eddies observed by high frequency radar: A new mechanism for delivering nutrients to kelp forests in the Southern California Bight, *Geophys. Res. Lett.*, **32**, L12604, doi:10.1029/2005GL023017.
- Batchelor, G. K., and I. Proudman (1954), The effect of rapid distortion of a fluid in turbulent motion, *Q. J. Mech. Appl. Math.*, **7**, 83–103.
- Chang, M.-S. (1969), Mass transport in deep-water long-crested random gravity waves, *J. Geophys. Res.*, **74**, 1515–1536.
- Craig, P. D., and M. L. Banner (1994), Modeling wave-enhanced turbulence in the ocean surface layer, *J. Phys. Oceanogr.*, **24**, 2546–2559.
- Craik, A. D. D. (1982), The generalized Lagrangian-mean equations and hydrodynamic stability, *J. Fluid Mech.*, **125**, 27–35.
- Crosby, D. S., L. C. Breaker, and W. H. Gemmill (1993), A proposed definition for vector correlation in Geophysics: Theory and application, *J. Atmos. Oceanic Technol.*, **10**, 355–367.
- Csanady, G. T. (1984), The free surface turbulent shear layer, *J. Phys. Oceanogr.*, **14**, 402–411.
- Dunlap, E., C. L. Tang, and C. K. Wang (2004), Comparison of model surface currents and drifter data from the Grand Banks, *Can. Tech. Rep. Hydrogr. Ocean Sci.*, **236**, 28 pp.
- Gerstner, F. J. (1804), *Theorie der Wellen*, Abhandl. Kgl. Böhm. Ges. Wiss., Prague.
- Grant, W. D., and O. S. Madsen (1979), Combined wave and current interaction with a rough bottom, *J. Geophys. Res.*, **84**, 1797–1808.
- Gray, D. E. (Ed.) (1972), *American Institute of Physics Handbook*, pp. 2–267, Am. Inst. of Phys., College Park, Md.
- Grimshaw, R. (1981), Mean flows generated by a progressing water wave packet, *J. Aust. Math. Soc.*, **B22**, 318–347.
- Groeneweg, J., and J. A. Battjes (2003), Three-dimensional wave effects on a steady current, *J. Fluid Mech.*, **478**, 325–343.
- Groeneweg, J., and G. Klopman (1998), Changes of the mean velocity profiles in the combined wave-current motion described in a GLM formulation, *J. Fluid Mech.*, **370**, 271–296.
- Han, G. (2000), Three-dimensional modeling of tidal currents and mixing quantities over the Newfoundland Shelf, *J. Geophys. Res.*, **105**, 11,407–11,422.
- Han, G., M. Ikeda, and P. C. Smith (1996), Oceanic tides over the Newfoundland and Scotian Shelves from TOPEX/POSEIDON altimetry, *Atmos. Ocean*, **34**, 589–604.
- Hasselmann, K. (1970), Wave-driven inertial oscillations, *Geophys. Fluid Dyn.*, **1**, 463–502.
- Hasselmann, K. (1974), On the spectral dissipation of ocean waves due to white capping, *Boundary Layer Meteorol.*, **6**, 107–127.
- Huang, N. E. (1971), Derivation of Stokes drift for a deep-water random gravity wave field, *Deep Sea Res.*, **18**, 255–259.
- Jenkins, A. D. (1986), A theory for steady and variable wind and wave induced currents, *J. Phys. Oceanogr.*, **16**, 1370–1377.
- Jenkins, A. D. (1987), Wind and wave induced currents in a rotating sea with depth-varying eddy viscosity, *J. Phys. Oceanogr.*, **17**, 938–951.
- Jenkins, A. D. (1989), The use of a wave prediction model for driving a near-surface current model, *Dtsch. Hydrogr. Z.*, **42**, 133–149.
- Jenkins, A. D., and F. Ardhuin (2004), Interaction of ocean waves and currents: How different approaches may be reconciled, paper presented at 14th International Offshore and Polar Engineering Conference, Int. Soc. of Offshore and Polar Eng., Toulon, France.
- Komen, G. J., L. Cavaleri, M. Donelan, K. Hasselmann, S. Hasselmann, and P. A. E. Janssen (1994), *Dynamics and Modelling of Ocean Waves*, 532 pp., Cambridge Univ. Press, New York.
- Lamb, H. (1932), *Hydrodynamics*, 6th ed., 738 pp., Cambridge University Press, New York.
- Liu, A. K., Y. Zhao, and M.-K. Hsu (2006), Ocean surface drift revealed by synthetic aperture radar images, *Eos Trans. AGU*, **87**, 61–72.
- Longuet-Higgins, M. S. (1953), Mass transport in water waves, *Philos. Trans. R. Soc., Ser. A*, **245**, 535–581.
- Longuet-Higgins, M. S., and R. W. Stewart (1960), Changes in the form of short gravity waves on long waves and tidal currents, *J. Fluid Mech.*, **8**, 565–583.
- Longuet-Higgins, M. S., and R. W. Stewart (1962), Radiation stress and mass transport in gravity waves with application to surf beats, *J. Fluid Mech.*, **13**, 481–504.
- Mastenbroek, C., V. K. Makin, M. H. Garat, and J. P. Giovanangeli (1996), Experimental evidence of the rapid distortion of turbulence in the air flow over water waves, *J. Fluid Mech.*, **318**, 273–302.
- McWilliams, J. C., P. P. Sullivan, and C.-H. Moeng (1997), Langmuir turbulence in the ocean, *J. Fluid Mech.*, **334**, 1–30.
- Mellor, G. (2002), Oscillatory bottom boundary layers, *J. Phys. Oceanogr.*, **32**, 3075–3088.
- Mellor, G. (2003), The three-dimensional current and surface wave equations, *J. Phys. Oceanogr.*, **33**, 1978–1999.
- Mellor, G. L., and A. F. Blumberg (2004), Wave breaking and ocean surface layer thermal response, *J. Phys. Oceanogr.*, **34**, 693–698.
- Mitsuyasu, H. (1968), On the growth of the spectrum of wind-generated waves, 1, *Rep. Res. Inst. Appl. Mech. Kyushu Univ.*, **16**, 459–482.
- Mitsuyasu, H. (1985), A note on the momentum transfer from wind to waves, *J. Geophys. Res.*, **90**, 3343–3345.
- Mitsuyasu, H., and T. Honda (1982), Wind induced growth of water waves, *J. Fluid Mech.*, **123**, 425–442.
- Paduan, J. D., P. M. Kosro, and S. M. Gleen (2004), A national coastal ocean high frequency radar system for the United States, *Mar. Technol. Soc. J.*, **38**, 76–82.
- Perrie, W., C. L. Tang, Y. Hu, and B. M. DeTracey (2003), The impact of waves on surface currents, *J. Phys. Oceanogr.*, **33**, 2126–2140.
- Pollard, R. T. (1970), Surface waves with rotation: an exact solution, *J. Geophys. Res.*, **75**, 5895–5898.
- Resio, D. T., C. E. Long, and C. L. Vincent (2004), Equilibrium-range constant in wind-generated wave spectra, *J. Geophys. Res.*, **109**, C01018, doi:10.1029/2003JC001788.
- Smith, J. A. (2006), Observed variability of ocean wave Stokes drift and the Eulerian response to passing groups, *J. Phys. Oceanogr.*, **36**, 1381–1402.
- Smith, P. C. (1992), Validation procedures for oil spill trajectory models, *Can. Tech. Rep. Hydrogr. Ocean Sci.* **140**, pp. 169–183, Fish. and Oceans Can., Ottawa.
- Smith, P. C., D. J. Lawrence, K. R. Thompson, J. Sheng, G. Verner, J. St. James, N. Bernier, and L. Feldman (1999), Improving the skill of search-and-rescue forecasts, *CMOS Bull.*, **26**, 119–129.
- Stacey, M. W. (1999), Simulation of the wind-forced near-surface circulation in Knight Inlet: A parameterization of the roughness length, *J. Phys. Oceanogr.*, **29**, 1363–1367.
- Stokes, G. G. (1847), On the theory of oscillatory waves, *Trans. Cambridge Philos. Soc.*, **8**, 441–455.
- Tang, C. L., Q. Gui, and I. Peterson (1996), Modeling the mean circulation of the Labrador Sea and the adjacent shelves, *J. Phys. Oceanogr.*, **26**, 1989–2010.
- Tang, C. L., Q. Gui, and B. M. DeTracey (1998), Barotropic response of the Labrador/Newfoundland shelf to a moving storm, *J. Phys. Oceanogr.*, **28**, 1152–1191.
- Teixeira, M. A. C., and S. E. Belcher (2002), On the distortion of turbulence by a progressive surface wave, *J. Fluid Mech.*, **458**, 229–267.
- Terray, E. A., M. A. Donelan, Y. C. Agrawal, W. M. Drennan, K. K. Kahma, A. J. Williams, P. A. Hwang, and S. A. Kitaigorodski (1996), Estimates of kinetic energy dissipation under breaking waves, *Phys. Oceanogr.*, **26**, 792–807.
- Thornton, E. B., and R. T. Guza (1986), Surf zone longshore currents and random waves: Field data and models, *J. Phys. Oceanogr.*, **16**, 1165–1178.
- Tolman, H. L. (2002), User manual and system documentation of Wave-watch III version 2.22, *Tech. Note 222*, 133 pp., NOAA, Silver Spring, Md. [Available at <http://polar.ncep.noaa.gov/waves>]

- Tolman, H. L., and D. V. Chalikov (1996), Source terms in a third-generation wind wave model, *J. Phys. Oceanogr.*, *26*, 2497–2518.
- Townsend, A. A. (1976), *The Structure of Turbulent Shear Flow*, 2nd ed., Cambridge Univ. Press, New York.
- Ullman, D. S., and D. L. Codiga (2004), Seasonal variation of a coastal jet in the Long Island Sound outflow region based on HF radar and Doppler current observations, *J. Geophys. Res.*, *109*, C07S06, doi:10.1029/2002JC001660.
- Ünlüata, Ü., and C. C. Mei (1970), Mass transport in water waves, *J. Geophys. Res.*, *75*, 7611–7618.
- Ursell, F. (1950), On the theoretical form of ocean swell on a rotating Earth, *Mon. Not. R. Astron. Soc.*, *6*, Geophys. Suppl., 1–8.
- WAMDI Group (1988), The WAM model—A third generation ocean wave prediction model, *J. Phys. Oceanogr.*, *18*, 1775–1810.
- Weber, J. E. (1983a), Steady wind- and wave-induced currents in the open ocean, *J. Phys. Oceanogr.*, *13*, 524–530.
- Weber, J. E. (1983b), Attenuated wave-induced drift in a viscous rotating ocean, *J. Fluid Mech.*, *137*, 115–129.
- Yao, T., C. L. Tang, and I. K. Peterson (2000a), Modeling the seasonal variation of sea ice in the Labrador Sea with a coupled multi-category ice model and the Princeton Ocean Model, *J. Geophys. Res.*, *105*, 1153–1165.
- Yao, T., C. L. Tang, T. Carrieres, and D. H. Tran (2000b), Verification of a coupled ice ocean forecasting system for the Newfoundland Shelf, *Atmos. Ocean*, *38*, 557–575.
- 
- B. M. DeTracey, Y. Hu, W. Perrie, P. C. Smith, C. L. Tang, and B. Toulany, Bedford Institute of Oceanography, Ocean Sciences Division, Fisheries and Oceans Canada, Dartmouth, Nova Scotia, Canada B2Y 4A2. (detraceyb@mar.dfo-mpo.gc.ca; huy@mar.dfo-mpo.gc.ca; perriew@mar.dfo-mpo.gc.ca; smithpc@mar.dfo-mpo.gc.ca; tangc@mar.dfo-mpo.gc.ca; toulanyb@mar.dfo-mpo.gc.ca)
- A. D. Jenkins, Geophysical Institute, University of Bergen & Bjerknes Centre for Climate Research, Allégaten 70, N-5007 Bergen, Norway. (alastair.jenkins@gfi.uib.no)